Unmanned Systems, Vol. 14, No. 1 (2026) 167–180
© World Scientific Publishing Company
DOI: 10.1142/S2301385025500876

Unmanned Systems
https://www.worldscientific.com/worldscinet/us

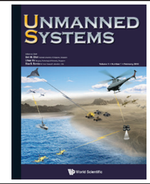

Safety-Critical Containment Control for Quadrotor Team Using Exponential Control Barrier Functions

Zheng Xia*, Mou Chen

College of Automation Engineering,
Nanjing University of Aeronautics and Astronautics, Nanjing, Jiangsu, China

In this work, the containment control problem for a quadrotor team is addressed in the presence of multiple dynamic leaders with unknown bounded time-varying inputs. Both safety-critical constraints and input constraints are considered. Specifically, a linear extended state observer (ESO) is employed to handle the uncertainty and disturbance. A distributed fixed-time observer is designed to estimate the reference signal requiring no global information. The proposed nominal controller can guarantee the formation geometric constraint in steady states. Moreover, safety certificates for collision-free in transient states is enforced by using exponential control barrier functions (ECBFs). A real-time quadratic programming (QP) problem is constructed to modify the nominal controller such that both safety constraint and input constraint can be satisfied. Finally, simulations and experiments illustrate the effectiveness of the algorithm.

Keywords: Containment control; quadrotor team; multiple constraints; safety-critical; ECBF.

1. Introduction

Over the past few decades, there has been a growing interest in the research of multi-agent systems (MAS) [1, 2]. The theory of MAS has been successfully employed in autonomous unmanned systems [3] like unmanned surface vehicles (USVs) [4], mobile robots [5], unmanned aerial vehicles (UAVs) [6]. Specifically, owing to the superiority in efficiency and robustness, the collaboration of UAV teams has various applications in military or civilian fields such as air combat [7], transportation [8], detection and forest fire monitoring [9]. Especially, quadrotor is a type of vertical take-off and landing (VTOL) UAV with the ability of agile flight [10]. Based on the above analysis, we can find several benefits and great potential of the coordinated control for quadrotors. Therefore, it's meaningful for people to give further investigation.

Through reviewing relevant works from control community, we summarize the following challenging issues:

- Formation maneuver for quadrotor teams. Since the UAVs always work in urban or wild environments, they should change the formation pattern in real time to adapt to the highly constrained environment.
- The existence of external disturbances and system uncertainties. These factors will affect the control performance of quadrotors.
- Multiple constraints on quadrotors especially safety constraint. In reality, the limitations of resource and capability make control design difficult. Moreover, we should ensure the safety of quadrotors strictly.

In earlier studies, formation control problems were dealt with mainly based on consensus protocols [11, 12]. In these cases, the formation configuration is time invariant. Then people started to pay attention to formation maneuver problem. Dong *et al.* proposed necessary and sufficient conditions to achieve the tracking of a predefined time-varying configuration subjected to switching topologies [13]. In [14], the time-varying formation problem of UAV

Received 6 March 2024; Revised 1 November 2024; Accepted 3 November 2024; Published 27 December 2024. This paper was recommended for publication in its revised form by editorial board member, Yi Dong.
Email Address: *SX2203169@nuaa.edu.cn*
*Correspondence author.

swarms was investigated, and a swarm platform experiment was presented. Recently, some new methods to achieve formation maneuver have been developed, which includes stress matrices [15, 16] and complex Laplacians [17, 18]. Zhao [19] employed affine transformations like scaling, shearing etc. to generate configurations with time-varying geometric properties, then the tracking control scheme was designed integrated with stress matrices. Moreover, containment control can be seen as a special type of formation. In this scenario, the agents not only need to follow the leaders, they are also steered in a convex hull-spanned by the leaders. This approach is useful to ensure the UAVs maneuvering in a safe region [20]. It is noteworthy that in these works, the leaders' input signal (e.g. the acceleration of a second-order system) will always appear in the control protocol for the followers. Therefore, people usually make assumptions that leaders' inputs are zero or the signals are known to all the followers [21, 22]. However, in most practical cases, leaders' inputs are time-varying and cannot been accessed by the followers in real time. Currently, only a few works consider this case [23]. Inspired by the condition, investigating the containment control problem with leaders' inputs unknown is one of the motivations of our work.

Many existing literature works on MAS investigated the problem based on an ideal model. However, for robotic systems like UAVs, etc., the external disturbances cannot be ignored [24]. A more practical model should be used to describe the dynamic. Thus, this work aims at tackling the negative affects of lumped disturbances for better performance of UAV teams.

In reality, there are always multiple constraints on the MAS. For instance, communication constraints, connectivity constraints, state constraints, energy constraints, etc. There are methods to deal with these constraints, respectively. Dynamic event-triggered (ET) mechanism was employed in MAS formation to reduce redundant data exchanges [25]. In [26, 27], distributed controller was designed for MAS subject to input constraints. Prescribed performance (PPC) [28] and barrier Lyapunov function (BLF) [29] can be used to guarantee the state constraints. Moreover, model predictive control (MPC) [30, 31] is a good strategy for MAS to achieve optimal performance while handling constraints. On the other hand, robotic systems like UAV teams are typical safety-critical systems, which means collision with obstacles or collision between agents should be avoided to ensure the safety. For quadrotors, downwash has considerable effects on their safety too [32]. Artificial potential field (APF) is popular in collision avoidance for UAVs, USVs [33]. However, APFs always have the problem of local optima, which reveals the limitation of this approach. It can be found that there are very few works simultaneously consider multiple constraints in one problem. On the other hand, the multiple constraints may contradict with each other. Therefore, the problem on how to realize a trade-off between the constraints appropriately is still open. Our work is motivated by this challenge.

Compared with the aforementioned methods, control barrier functions (CBFs)-based safety certificate is a novel and powerful one. Safety is ensured through enforcing the forward invariance of the safety set. Reciprocal control barrier functions (RCBFs) and zeroing control Barrier functions (ZCBFs) were investigated by Ames *et al.* in [34]. In their work, a CBF-based QP optimization framework was constructed and has been successfully applied in adaptive cruise control (ACC). Employing ZCBF, collision avoidance and connectivity maintenance were achieved for second-order MAS in [35]. The safety control for USVs using CBFs with disturbance has been studied in [36]. However, we find that there is little research on exponential control barrier functions (ECBFs) [37], which is more powerful for high order systems. In our work, we will try to apply this method on quadrotor teams for ensuring safety.

Based on the above analysis, this work aims at the containment control for quadrotor teams. Key problems considered are summarized as follows. The first problem is how to realize the control objective when leaders' control input is unknown. The second one is how to tackle the negative affects of disturbances and uncertainties to maintain system performance. The final one is how to ensure that the multiple constraints especially safety constraints are satisfied for the quadrotors. Main contributions are listed in the following:

- Containment formation maneuver can be achieved in the presence of leaders with unknown time-varying accelerations. There is no need for acceleration measurements and acceleration feedback. A fixed time observer is constructed for controller design. Moreover, disturbance and uncertainties will be estimated and compensated in this problem.
- Multiple constraints are handled such as safety-critical constraints and input constraints. Besides the distance-based collision-free constraints [35], the effects of downwash are also considered in the work for the safety of quadrotors.
- A decentralized CBF-based QP method is proposed for the optimal controller, which makes a trade-off between soft constraints and hard constraints. Compared with the existing algorithms commonly used [38], an ECBF rather than a ZCBF is employed for the quadrotor team.

The remaining part of this paper is organized as follows. In Sec. 2, preliminaries and problem formulation are given, including models, control objectives and lemmas. In Sec. 3, we propose the nominal controller and modified controller to handle the problems. Simulations and experiments are shown in Secs. 4 and 5, respectively. Finally, we give the conclusion and discussion of this work in Sec. 6.

2. Preliminaries and Problem Formulation

2.1. *Notations*

First, we will introduce the mathematical symbols used throughout this paper. Let $1_n = [1, 1, \dots, 1]^T \in \mathbb{R}^n$ for simplicity, while I_n represents an nth order identity matrix and O is a zero matrix. $A^{[j]}$ means the jth row of matrix A. $\mathrm{sgn}(\cdot)$ is the sign function. When $c = [c_1, c_2, \dots, c_n]^T \in \mathbb{R}^n$, $\mathrm{sig}^a(c) = [\mathrm{sig}^a(c_1), \dots, \mathrm{sig}^a(c_n)]^T \in \mathbb{R}^n$. Specifically, $\mathrm{sig}^a(c_i) = |c_i|^a \mathrm{sgn}(c_i)$, where the superscript $a \in \mathbb{R}$ means a power exponent. $\mathrm{diag}\{q_1, \dots, q_N\}$ is a diagonal matrix and $q_1, \dots, q_N$ are entries on its principal diagonal. $\otimes$ is the symbol of Kronecker product. $\lambda_{\max}(\cdot)$ and $\lambda_{\min}(\cdot)$ denote the maximum and minimum eigenvalues of a matrix, respectively.

2.2. *Quadrotor dynamics*

The quadrotor can be treated as a 6-degree-of-freedom (DoF) rigid. Its motion can be defined in a inertial frame $\mathcal{W}$ and a body-fixed frame $\mathcal{B}$. Denote $R \in SO(3)$ as the rotation matrix from $\mathcal{B}$ to $\mathcal{W}$. $x, v \in \mathbb{R}^3$ are position and linear velocity of the center of mass (CoM) in $\mathcal{W}$. $\Omega \in \mathbb{R}^3$ is angular velocity defined in $\mathcal{B}$. Then for the ith quadrotor in the set $F = \{1, 2, \dots, N\}$, we have a nominal model in the following [39]:

$$\begin{aligned} \dot{x}_i &= v_i \\ m_i \dot{v}_i &= f_i R_i e_3 - m_i g e_3 \\ \dot{R}_i &= R_i \Omega_i^{\wedge} \\ J_i \dot{\Omega}_i &= \tau_i - \Omega_i \times J_i \Omega_i, \quad i \in F, \end{aligned} \tag{1}$$

where $m_i \in \mathbb{R}$ and $J_i \in \mathbb{R}^{3\times 3}$ are total mass and inertial matrix, respectively. e_3 represents a direction vector $[0, 0, 1]^T$. The direction of gravity is along $-\boldsymbol{Z}_{\mathcal{W}}$. g denotes the gravity acceleration. $(\cdot)^{\wedge}$ is a map: $\mathbb{R}^3 \to SO(3)$. f_i and τ_i are the thrust and torque generated by the propellers which can be seen as the control inputs, where f_i aligns the body axis $\boldsymbol{Z}_{\mathcal{B}}$.

It can be seen that quadrotor has underactuated and highly coupled dynamic. A quadrotor is equipped with four motors which means only 4 DoF can be considered simultaneously. Generally, people focus on the translation control for quadrotors in formation. Moreover, the yaw angle ψ can be set independently for quadrotor during flight. Therefore, $\Upsilon = [x^T, \psi]^T \in \mathbb{R}^3 \times SO(2)$ are chosen as the 4 DoF to be controlled [10].

Specifically, from the ideal model in (1), a more realistic one can be constructed for the quadrotor's translation dynamic

$$\begin{aligned} \dot{x}_i &= v_i \\ \dot{v}_i &= u_i + \bar{\boldsymbol{g}} + \rho_i v_i + \Delta_i, \quad i \in F, \end{aligned} \tag{2}$$

where $\bar{\boldsymbol{g}} = [0, 0, -g]^T$, $\rho_i v_i$ represents modeled the aerodynamic drag effect. $\rho_i = \mathrm{diag}\{\rho_{i,1}, \rho_{i,2}, \rho_{i,3}\}$, and the parameters can be identified through experiment data. Δ_i denotes the lumped uncertainties and disturbance. For the convenience of analysis, we organize the variables as a compact form. Let $\boldsymbol{x} = [x_1^T, x_2^T, \dots, x_N^T]^T \in \mathbb{R}^{3N}$, $\boldsymbol{v} = \dot{\boldsymbol{x}} = [v_1^T, v_2^T, \dots, v_N^T]^T \in \mathbb{R}^{3N}$.

In (2), we define a control input u_i. From u_i, one can derive the desired thrust $\boldsymbol{f}_{id}$, respectively. In the following, we introduce how to compute the desired attitude [39]. First, the $\boldsymbol{Z}$ axis of $\mathcal{B}$ can be directed derived via $\boldsymbol{f}_{id}$

$$\boldsymbol{Z}_{id} = \frac{\boldsymbol{f}_{id}}{\|\boldsymbol{f}_{id}\|}. \tag{3}$$

Next, for a given yaw angle ψ_{id}, we construct a vector $\boldsymbol{X}_{ic} = [\cos\psi_{id}, \sin\psi_{id}, 0]^T$. Then we have

$$\begin{aligned} \boldsymbol{Y}_{id} &= \frac{\boldsymbol{Z}_{id} \times \boldsymbol{X}_{ic}}{\|\boldsymbol{Z}_{id} \times \boldsymbol{X}_{ic}\|}, \\ \boldsymbol{X}_{id} &= \boldsymbol{Y}_{id} \times \boldsymbol{Z}_{id}. \end{aligned} \tag{4}$$

The desired attitude is $R_{id} = [\boldsymbol{X}_{id}\ \boldsymbol{Y}_{id}\ \boldsymbol{Z}_{id}]$. Assuming that the quadrotor has a underlying controller for the attitude control [40]. In this paper, we will not discuss the rotation control, i.e. how to design the torque.

2.3. *Leaders' signal*

There will be multiple leaders in the containment-formation scenario. Their dynamics are generated by a double integrator [23]

$$\begin{aligned} \dot{p}_j(t) &= q_j(t) \\ \dot{q}_j(t) &= r_j(t), \quad j \in L, \end{aligned} \tag{5}$$

where $L = \{N+1, \dots, N+M\}$ is the set of leaders. $p_j(t)$ and $q_j(t)$ are position and velocity signal. While $r_j(t)$ is an unknown bounded signal. $\|r_j(t)\|_\infty \le \bar{r}$, $\bar{r}$ is a constant known to the followers. Similarly, let $\boldsymbol{p} = [p_{N+1}^T, p_{N+2}^T, \dots, p_{N+M}^T]^T \in \mathbb{R}^{3M}$, $\boldsymbol{q} = [q_{N+1}^T, q_{N+2}^T, \dots, q_{N+M}^T]^T \in \mathbb{R}^{3M}$, respectively.

Remark 2.1. The leaders' signal will generate a safe zone in a convex hull for the follower quadrotors. In this paper, there are virtual leaders. Compared with zero acceleration or constant acceleration, leaders with time-varying unknown inputs are more general. It allows formation maneuver such that the quadrotors can adapt to the changing environment.

Remark 2.2. Unless otherwise stated, the signals in this paper which represent coordinate, velocity, input, disturbance, etc. are all time-varying. However, for the brevity, we will omit the time argument (t) in most cases.

2.4. *Control objective*

In the containment control problem of this paper, the multiple constraints to be satisfied are described in the following.

2.4.1. *Geometric constraints*

The quadrotors are contained in the convex hull spanned by leaders, which can be formulated as

$$\lim_{t\to\infty} \left\| x_i - \sum_{j=N+1}^{N+M} k_{ij} p_j \right\| \le \varepsilon_i, \quad i \in F, \tag{6}$$

where the coefficients $k_{ij} \ge 0$, and $\sum_{j=N+1}^{N+M} k_{ij} = 1$. $\varepsilon_i > 0$ is a small scalar.

2.4.2. *Safety-critical constraints*

The inter-collision between the quadrotors should be avoided while flying or transforming the formation.

$$\|\Lambda^{-1}(x_i - x_j)\| \ge D_s, \quad i,j \in F, \tag{7}$$

where Λ is a scaling matrix [32], $\Lambda = \mathrm{diag}\{1, 1, l\}$, $l > 1$. D_s denotes the safety distance between 2 quadrotors i and j.

2.4.3. *Input constraints*

Actually, there is always a limit on a quadrotor's maneuver capability and control input. That is

$$\|u_i\|_\infty \le \alpha_i, \quad i \in F, \tag{8}$$

where α_i is a positive constant.

Remark 2.3. Let us consider the downwash effects generated by the rotors. Inspired by Hönig *et al.* [41], the collision volume of a UAV is expanded into a ellipsoid in the vertical axis. In this way, the safety of a quadrotor can be guaranteed when flying underneath another, as shown in Fig. 1.

Remark 2.4. Among the above constraints, the latter two are considered as hard constraints which should be strictly satisfied at all time. While the first one is a soft constraint.

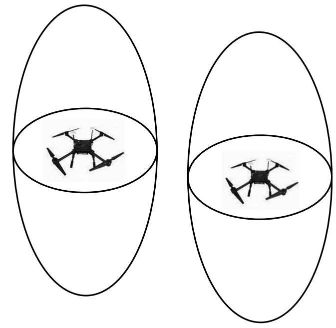

Fig. 1. Ellipsoid volume for quadrotors.

We hope that the containment error is small as possible. It can be violated sometimes when contradicting the hard constraints.

2.5. *Graph theory*

A graph $\mathcal{G}(\mathcal{V}, \mathcal{E}, \mathcal{A})$ will be used to describe the communication topology [42]. $\mathcal{V} = \{1, 2, \ldots, N+M\}$ is the node set, $\mathcal{E}$ is the edge set and $\mathcal{A} = [a_{ij}] \in \mathbb{R}^{(N+M)\times(N+M)}$ denotes the adjacency matrix of $\mathcal{G}$. If node i can receive information from node j, j is a neighbor of i. We have $(i,j) \in \mathcal{E}$, $a_{ij} > 0$. Otherwise, $a_{ij} = 0$. $d_i = \sum_{j=1}^{N+M} a_{ij}$ is called indegree. We have the indegree matrix $D = \mathrm{diag}\{d_1, \ldots, d_{N+M}\}$. Then the Laplacian matrix of $\mathcal{G}$ is given by $\mathcal{L} = \mathcal{D} - \mathcal{A}$.

In this paper, the leaders only send information and don't receive information. The interactions between follower quadrotors are undirected. Assuming that for each quadrotor, there exists at least one virtual leader which has a path to it. Then the Laplacian matrix $\mathcal{L}$ can be divided into blocks, which can be written as

$$\mathcal{L} = \begin{bmatrix} \mathcal{T}_1 & \mathcal{T}_2 \\ \mathcal{O}_1 & \mathcal{O}_2 \end{bmatrix} \in \mathbb{R}^{(N+M)\times(N+M)},$$

where $\mathcal{T}_1 \in \mathbb{R}^{N\times N}, \mathcal{T}_2 \in \mathbb{R}^{N\times M}, \mathcal{O}_1 \in \mathbb{R}^{M\times N}, \mathcal{O}_2 \in \mathbb{R}^{M\times M}$. Here, we have the following properties [43]. $\mathcal{T}_1$ is a symmetric and positive definite matrix. The entries of $-\mathcal{T}_1^{-1}\mathcal{T}_2$ are nonnegative. In each row of $-\mathcal{T}_1^{-1}\mathcal{T}_2$, the sum of the entries is 1. That is

$$-\mathcal{T}_1^{-1}\mathcal{T}_2^{[j]} \cdot 1_M = 1, \quad j = 1, \ldots, N. \tag{9}$$

2.6. *Lemmas*

Aiming at the control objectives above, some useful lemmas are introduced in this subsection.

Lemma 2.5. *Consider an affine dynamic system* [34, 37] *as follows:*

$$\dot{x} = f(x) + g(x)u \tag{10}$$

where $x \in \mathbb{R}^n$, $u \in \mathbb{R}^m$. Given a safety set

$$\mathcal{C} = \{x \in \mathbb{R}^n | h(x) \geq 0\}, \tag{11}$$

which is defined on the function $h : \mathbb{R}^n \to \mathbb{R}$. The function h has a relative degree of s. $h(x)$ is a exponential control barrier function (ECBF) defined on $\mathcal{C}$ if we can find $K \in \mathbb{R}^{1\times s}$ which satisfies

$$\sup_{u\in U}[L_f^s h(x) + L_g L_f^{s-1} h(x) + K\eta] \geq 0 \tag{12}$$

and $h(x) \geq C_s e^{A_s t}\eta(x_0) \geq 0$ when $h(x_0) \geq 0$, where $A_s = F_s - G_s K$, $C_s = [1, 0, \dots, 0]$, $\eta = [h(x), \dot{h}(x), \dots, h^{(s-1)}(x)]^T$. The matrices $F_s \in \mathbb{R}^{s\times s}$, $G_s \in \mathbb{R}^{s\times 1}$ are derived from the controllable canonical form

$$F_s = \begin{bmatrix} 0 & 1 & \cdots & 0 \\ \vdots & \ddots & \ddots & \vdots \\ 0 & & \ddots & 1 \\ 0 & \cdots & & 0 \end{bmatrix}, \quad G_s = \begin{bmatrix} 0 \\ \vdots \\ 1 \end{bmatrix}. \tag{13}$$

The vector K should be selected to ensure that A_s is Hurwitz. For the ECBF, the admissible control space $\mathcal{U}(x)$ is defined as

$$\mathcal{U}(x) = \{u | L_f^s h(x) + L_g L_f^{s-1} h(x) + K\eta \geq 0\}, \quad x \in \mathcal{C}. \tag{14}$$

For the safety set (11) and an associated ECBF h, with the system's initial state, $x_0 \in \mathcal{C}$. The forward invariance of $\mathcal{C}$ can be rendered using any controller $u \in \mathcal{U}(x)$.

This lemma is about safety control. It will be used for ensuring the collision avoidance for quadrotors.

Lemma 2.6. *For any $\theta_1, \theta_2, \dots, \theta_N \geq 0$ [44], if $0 < p \leq 1$, we have*

$$\sum_{i=1}^{N} \theta_i^p \geq \left(\sum_{i=1}^{N} \theta_i\right)^p$$

if $p > 1$, the following inequality holds:

$$\sum_{i=1}^{N} \theta_i^p \geq N^{1-p}\left(\sum_{i=1}^{N} \theta_i\right)^p.$$

These inequalities will be utilized in the process of Lyapunov function for proof.

Lemma 2.7. ([45]) *Consider the following system:*

$$\dot{x} = f(t, x), \quad x(0) = x_0$$

If there exists a continuous function $V(x) : R^n \to R_+ \cup \{0\}$, which satisfies

- *$V(x) = 0 \Longleftrightarrow x = 0$;*
- *$\dot{V}(x) \leq -k_\alpha V^{l_1}(x) - k_\beta V^{l_2}(x)$,*

where $k_\alpha, k_\beta > 0$, $l_1 > 1$, $0 < l_2 < 1$. Then the system is globally fixed-time stable. The settling time has an upper bound:

$$T \leq T_{\max} = \frac{1}{k_\alpha(l_1 - 1)} + \frac{1}{k_\beta(1 - l_2)}. \tag{15}$$

In this work, we will design an observer with faster convergence rate based on this lemma.

3. Main Results

3.1. *ESO design for estimation*

Since the lumped uncertainties and disturbances have physical limitations, it is reasonable to assume that Δ_i and $\dot{\Delta}_i$ are bounded. Namely,

$$\|\Delta_i\| \leq \bar{\Delta}; \quad \|\dot{\Delta}_i\| \leq \bar{\dot{\Delta}}. \tag{16}$$

Now, we can extend Δ_i as an additional state for the system. Motivated by Yue *et al.* [46], we will use an ESO to estimate the unknown item. The design is given below, in which $(\hat{\cdot})$ represents the estimation value

$$\begin{aligned} \dot{\hat{x}}_{i,\kappa} &= \hat{v}_{i,\kappa} + 3\omega_{i,\kappa}(x_{i,\kappa} - \hat{x}_{i,\kappa}) \\ \dot{\hat{v}}_{i,\kappa} &= u_{i,\kappa} + \bar{\boldsymbol{g}}_\kappa + \rho_{i,\kappa} v_{i,\kappa} + \hat{\Delta}_{i,\kappa} + 3\omega_{i,\kappa}^2(x_{i,\kappa} - \hat{x}_{i,\kappa}) \\ \dot{\hat{\Delta}}_{i,\kappa} &= \omega_{i,\kappa}^3(x_{i,\kappa} - \hat{x}_{i,\kappa}). \quad \kappa = 1, 2, 3. \ i \in F, \end{aligned} \tag{17}$$

where the subscript κ denotes the κth entry of a vector. $\boldsymbol{\omega}_i = \mathrm{diag}\{\omega_{i,1}, \omega_{i,2}, \omega_{i,3}\}$ is the adjustable parameter of the ESO. We obtain the dynamics of estimation error $(\tilde{\cdot})$,

$$\begin{aligned} \dot{\tilde{x}}_{i,\kappa} &= \tilde{v}_{i,\kappa} - 3\omega_{i,\kappa}\tilde{x}_{i,\kappa}, \\ \dot{\tilde{v}}_{i,\kappa} &= \tilde{\Delta}_{i,\kappa} - 3\omega_{i,\kappa}^2\tilde{x}_{i,\kappa}, \\ \dot{\tilde{\Delta}}_{i,\kappa} &= \dot{\Delta}_{i,\kappa} - \omega_{i,\kappa}^3\tilde{x}_{i,\kappa}. \end{aligned} \tag{18}$$

Furthermore, let $\sigma_{i,\kappa} = [\tilde{x}_{i,\kappa}, \frac{\tilde{v}_{i,\kappa}}{\omega_{i,\kappa}}, \frac{\tilde{\Delta}_{i,\kappa}}{\omega_{i,\kappa}^2}]^T$, then

$$\dot{\sigma}_{i,\kappa} = \omega_{i,\kappa}\underbrace{\begin{bmatrix} -3 & 1 & 0 \\ -3 & 0 & 1 \\ -1 & 0 & 0 \end{bmatrix}}_{A_e}\sigma_{i,\kappa} + \begin{bmatrix} 0 \\ 0 \\ 1 \end{bmatrix}\frac{\dot{\Delta}_{i,\kappa}}{\omega_{i,\kappa}^2}. \tag{19}$$

The system matrix A_e is Hurwitz and $\dot{\Delta}_{i,\kappa}$ is bounded. According to Cao *et al.* [47], the estimation error is bounded. There will be a finite time T_1 such that

$$\|\tilde{\boldsymbol{\Delta}}\| \leq \zeta_1, \quad t \geq T_1, \tag{20}$$

where $\tilde{\boldsymbol{\Delta}} = [\tilde{\Delta}_1^T, \dots, \tilde{\Delta}_N^T]^T$, and the upper bound ζ_1 will decrease through increasing $\omega_{i,\kappa}$.

3.2. *Fixed-time observer design*

According to the property of communication graph in (9), we can find that if the following condition holds:

$$\lim_{t\to\infty} \|\boldsymbol{x} - (-\mathcal{T}_1^{-1}\mathcal{T}_2 \otimes I_3)\boldsymbol{p}\| \le \varepsilon, \tag{21}$$

the containment control objective (6) will be achieved. Here, we denote

$$\boldsymbol{x}_d = (-\mathcal{T}_1^{-1}\mathcal{T}_2 \otimes I_3)\boldsymbol{p}, \tag{22}$$

which means $\boldsymbol{x}_d = [x_{1d}^T, x_{2d}^T, \ldots, x_{Nd}^T]^T$ is the desired trajectory for the following quadrotors in the containment control. However, the reference signal $\boldsymbol{x}_d$ contains global information such as topology matrix $\mathcal{T}_1$, $\mathcal{T}_2$, and leaders' location $\boldsymbol{p}$. Moreover, the leaders' dynamics (5) also have uncertainties. In other words, in the distributed framework, the reference trajectories (22) cannot be employed in the controller design directly.

Considering the above problem, here we design a fixed-time observer (FTO) for the following quadrotors to estimate the desired signal in a distributed way. From (22), we construct $\boldsymbol{v}_d = \dot{\boldsymbol{x}}_d = [v_{1d}^T, v_{2d}^T, \ldots, v_{Nd}^T]^T$. Define $\hat{v}_{id}$ as the estimation of v_{id}. Synchronization error of the estimation is given by

$$e_i = \sum_j a_{ij}(\hat{v}_{id} - \hat{v}_{jd}), \quad i \in F,\ j \in L \cup F. \tag{23}$$

Remark 3.1. For $j \in L$, $\hat{v}_{jd} = q_j$.

Then the FTO for quadrotor i is designed as

$$\dot{\hat{v}}_{id} = -k_1 \mathrm{sig}^a(e_i) - k_2 \mathrm{sgn}(e_i), \quad i \in F, \tag{24}$$

where $a > 1$, and k_1, k_2 are positive parameters to be designed. Denote $\hat{\boldsymbol{v}}_d = [\hat{v}_{1d}^T, \hat{v}_{2d}^T, \ldots, \hat{v}_{Nd}^T]^T$.

Let $\boldsymbol{e} = [e_1^T, e_2^T, \ldots, e_N^T]^T$. By using the property of communication topology, we can obtain

$$\begin{aligned}\boldsymbol{e} &= (\mathcal{T}_1 \otimes I_3)\hat{\boldsymbol{v}}_d + (\mathcal{T}_2 \otimes I_3)\boldsymbol{q}\\ &= (\mathcal{T}_1 \otimes I_3)[\hat{\boldsymbol{v}}_d - (-\mathcal{T}_1^{-1}\mathcal{T}_2 \otimes I_3)\boldsymbol{q}]\\ &= (\mathcal{T}_1 \otimes I_3)(\hat{\boldsymbol{v}}_d - \boldsymbol{v}_d)\\ &= (\mathcal{T}_1 \otimes I_3)\tilde{\boldsymbol{v}}_d,\end{aligned} \tag{25}$$

where $\tilde{\boldsymbol{\nu}}_d = \hat{\boldsymbol{v}}_d - \boldsymbol{v}_d$ represents the estimation error.

Then we give the design of parameters and stability analysis in the following theorem.

Theorem 3.2. *By choosing $k_1 > 0$, $k_2 > \bar{r}$, the desired signal can be estimated accurately in fixed-time.*

Proof. Construct a Lyapunov function:

$$V_1 = \frac{1}{2}\tilde{\boldsymbol{v}}_d^T(\mathcal{T}_1 \otimes I_3)^T\tilde{\boldsymbol{v}}_d. \tag{26}$$

By invoking (24) and (25), the time derivative of V_1 is

$$\begin{aligned}\dot{V}_1 &= \tilde{\boldsymbol{v}}_d^T(\mathcal{T}_1 \otimes I_3)^T\dot{\tilde{\boldsymbol{v}}}_d\\ &= \tilde{\boldsymbol{v}}_d^T(\mathcal{T}_1 \otimes I_3)^T(-k_1\mathrm{sig}^a(\boldsymbol{e}) - k_2\mathrm{sgn}(\boldsymbol{e}) - \dot{\boldsymbol{v}}_d)\\ &= -k_1\boldsymbol{e}^T\mathrm{sig}^a(\boldsymbol{e}) - k_2\boldsymbol{e}^T\mathrm{sgn}(\boldsymbol{e}) + \boldsymbol{e}^T(\mathcal{T}_1^{-1}\mathcal{T}_2 \otimes I_3)\dot{\boldsymbol{q}}\\ &= -k_1\sum_i |\boldsymbol{e}^{[i]}|^{a+1} - k_2\|\boldsymbol{e}\|_1 + \boldsymbol{e}^T(\mathcal{T}_1^{-1}\mathcal{T}_2 \otimes I_3)\dot{\boldsymbol{q}}.\end{aligned} \tag{27}$$

The following inequality of vector norms always holds:

$$\|\boldsymbol{e}\|_2 \le \|\boldsymbol{e}\|_1 \tag{28}$$

$$\begin{aligned}\boldsymbol{e}^T(\mathcal{T}_1^{-1}\mathcal{T}_2 \otimes I_3)\dot{\boldsymbol{q}} &\le \|\boldsymbol{e}\|_1 \cdot \|(\mathcal{T}_1^{-1}\mathcal{T}_2 \otimes I_3)\dot{\boldsymbol{q}}\|_\infty\\ &= \bar{r}\cdot\|\boldsymbol{e}\|_1.\end{aligned} \tag{29}$$

By considering (28), (29), we can obtain

$$\begin{aligned}\dot{V}_1 &\le -k_1N^{\frac{1-a}{2}}\|\boldsymbol{e}\|_2^{a+1} - (k_2 - \bar{r})\|\boldsymbol{e}\|_1,\\ &\le -k_1N^{\frac{1-a}{2}}\|\boldsymbol{e}\|_2^{a+1} - (k_2 - \bar{r})\|\boldsymbol{e}\|_2.\end{aligned} \tag{30}$$

Furthermore,

$$\begin{aligned}V_1 &= \frac{1}{2}\tilde{\boldsymbol{v}}_d^T(\mathcal{T}_1 \otimes I_3)^T\tilde{\boldsymbol{v}}_d\\ &\le \frac{1}{2}\lambda_{\max}(\mathcal{T}_1)\|\tilde{\boldsymbol{v}}_d\|_2^2,\end{aligned} \tag{31}$$

$$\begin{aligned}\|\boldsymbol{e}\|_2 &= \|(\mathcal{T}_1 \otimes I_3)\tilde{\boldsymbol{v}}_d\|_2\\ &= \sqrt{\tilde{\boldsymbol{v}}_d^T(\mathcal{T}_1 \otimes I_3)^T(\mathcal{T}_1 \otimes I_3)\tilde{\boldsymbol{v}}_d}\\ &\ge \sqrt{\lambda_{\min}^2(\mathcal{T}_1)\|\tilde{\boldsymbol{v}}_d\|_2^2}\\ &\ge \lambda_{\min}(\mathcal{T}_1)\sqrt{\frac{2}{\lambda_{\max}(\mathcal{T}_1)}}V_1^{\frac{1}{2}}.\end{aligned} \tag{32}$$

By substituting into (30), one has

$$\begin{aligned}\dot{V}_1 &\le -\underbrace{k_1N^{\frac{1-a}{2}}\lambda_{\min}^{a+1}(\mathcal{T}_1)\sqrt{\frac{2}{\lambda_{\max}(\mathcal{T}_1)}}^{\,a+1}}_{\mu_1}V_1^{\frac{a+1}{2}}\\ &\quad - \underbrace{(k_2 - \bar{r})\lambda_{\min}(\mathcal{T}_1)\sqrt{\frac{2}{\lambda_{\max}(\mathcal{T}_1)}}}_{\mu_2}V_1^{\frac{1}{2}}\\ &= -\mu_1V_1^{\frac{a+1}{2}} - \mu_2V_1^{\frac{1}{2}}.\end{aligned} \tag{33}$$

According to Lemma 2.7, the estimation error will converge to zero in fixed time, with the settling time

$$T_2 = \frac{2}{\mu_1(a-1)} + \frac{2}{\mu_2}. \tag{34}$$

We have $\|\tilde{\boldsymbol{v}}_d\| \le \zeta_2$. For $t > T_2$, $\|\tilde{\boldsymbol{v}}_d\| = 0$. This completes the proof. □

3.3. *Nominal controller design*

The quadrotors can estimate the reference signal precisely using the FTO, and the uncertainties can be estimated and compensated via the ESO. Based on the two observers, we first design a nominal controller to guarantee the control objective (21) at steady states. The backstepping-based scheme has the following steps:

Step 1: Define the tracking error $z_{1i} = x_i - x_{id}$, and $\boldsymbol{z}_1 = [z_{11}^T, z_{12}^T, \ldots, z_{1N}^T]^T$. Just like e_i given above, define

$$z_{2i} = \sum_j a_{ij}(x_i - x_j), \quad i \in F, j \in L \cup F, \tag{35}$$

where $x_j = p_j$ ($j \in L$). Let $\boldsymbol{z}_2 = [z_{21}^T, z_{22}^T, \ldots, z_{2N}^T]^T$. Similar to (25), we have

$$\begin{aligned} \boldsymbol{z}_2 &= (\mathcal{T}_1 \otimes I_3)\boldsymbol{x} + (\mathcal{T}_2 \otimes I_3)\boldsymbol{p} \\ &= (\mathcal{T}_1 \otimes I_3)[\boldsymbol{x} - (-\mathcal{T}_1^{-1}\mathcal{T}_2 \otimes I_3)\boldsymbol{p}] \\ &= (\mathcal{T}_1 \otimes I_3)(\boldsymbol{x} - \boldsymbol{x}_d) \\ &= (\mathcal{T}_1 \otimes I_3)\boldsymbol{z}_1. \end{aligned} \tag{36}$$

We know $\mathcal{T}_1$ is nonsingular, which means the boundedness of $\boldsymbol{z}_1$ and $\boldsymbol{z}_2$ is equivalent.

Step 2: Construct a Lyapunov function of $\boldsymbol{z}_1$ as follows:

$$V_2 = \frac{1}{2}\boldsymbol{z}_1^T(\mathcal{T}_1 \otimes I_3)^T\boldsymbol{z}_1, \tag{37}$$

and one has

$$\begin{aligned} \dot{V}_2 &= \boldsymbol{z}_1^T(\mathcal{T}_1 \otimes I_3)^T\dot{\boldsymbol{z}}_1 \\ &= \boldsymbol{z}_2^T(\dot{\boldsymbol{x}} - \dot{\boldsymbol{x}}_d) \\ &= \boldsymbol{z}_2^T(\boldsymbol{v} - \boldsymbol{v}_d). \end{aligned} \tag{38}$$

Step 3: Based on the analysis of V_2 and $\dot{V}_2$, here we design a virtual velocity signal $\boldsymbol{v}^* = [{v_1^*}^T, {v_2^*}^T, \ldots, {v_N^*}^T]^T$,

$$\boldsymbol{v}^* = -k_3\boldsymbol{z}_2 + \hat{\boldsymbol{v}}_d. \tag{39}$$

with $k_3 > 0$ as a parameter to be designed.

Step 4: Then define another error variable $\boldsymbol{z}_3 = [z_{31}^T, z_{32}^T, \ldots, z_{3N}^T]^T$,

$$\boldsymbol{z}_3 = \boldsymbol{v} - \boldsymbol{v}^*. \tag{40}$$

Finally, we give the nominal controller $\bar{\boldsymbol{u}} = [\bar{u}_1^T, \bar{u}_2^T, \ldots, \bar{u}_N^T]^T$. For quadrotor i:

$$\bar{u}_i = -\bar{\boldsymbol{g}} - \rho_i v_i - \hat{\Delta}_i - z_{2i} - k_4 z_{3i} + \dot{v}_i^*, \tag{41}$$

where $k_4 > 0$ is a parameter to be given.

Remark 3.3. Only v_{id} and not x_{id} is estimated. For quadrotor i, z_{1i} is still unknown while z_{2i} is available in the controller design.

Now, we show the parameters' selection and stability analysis of the controller in the following theorem.

Theorem 3.4. *The objective of containment control* (21) *can be achieved via the proposed nominal controller if we choose the parameters satisfying*

$$\begin{aligned} &\nu_1, \nu_2 > 0, \\ &k_3 > \frac{1}{2}\nu_1, \\ &k_4 > \frac{1}{2}\nu_2. \end{aligned} \tag{42}$$

Proof. The third Lyapunov function is constructed as follows:

$$V_3 = V_2 + \frac{1}{2}\boldsymbol{z}_3^T\boldsymbol{z}_3. \tag{43}$$

By taking the derivative, substitute (38), (39) and (41) into it

$$\begin{aligned} \dot{V}_3 &= \boldsymbol{z}_2^T(\boldsymbol{z}_3 - k_3\boldsymbol{z}_2 + \tilde{\boldsymbol{v}}_d) + \boldsymbol{z}_3^T(\tilde{\boldsymbol{\Delta}} - \boldsymbol{z}_2 - k_4\boldsymbol{z}_3 + \dot{\boldsymbol{v}}^* - \dot{\boldsymbol{v}}^*) \\ &= \boldsymbol{z}_2^T(\boldsymbol{z}_3 - k_3\boldsymbol{z}_2) + \boldsymbol{z}_2^T\tilde{\boldsymbol{v}}_d + \boldsymbol{z}_3^T(-\boldsymbol{z}_2 - k_4\boldsymbol{z}_3) + \boldsymbol{z}_3^T\tilde{\boldsymbol{\Delta}} \\ &= -k_3\boldsymbol{z}_2^T\boldsymbol{z}_2 + \boldsymbol{z}_2^T\tilde{\boldsymbol{v}}_d - k_4\boldsymbol{z}_3^T\boldsymbol{z}_3 + \boldsymbol{z}_3^T\tilde{\boldsymbol{\Delta}} \\ &\leq -k_3\boldsymbol{z}_2^T\boldsymbol{z}_2 + \frac{\nu_1}{2}\boldsymbol{z}_2^T\boldsymbol{z}_2 + \frac{1}{2\nu_1}\tilde{\boldsymbol{v}}_d^T\tilde{\boldsymbol{v}}_d - k_4\boldsymbol{z}_3^T\boldsymbol{z}_3 + \frac{\nu_2}{2}\boldsymbol{z}_3^T\boldsymbol{z}_3 \\ &\quad + \frac{1}{2\nu_2}\tilde{\boldsymbol{\Delta}}^T\tilde{\boldsymbol{\Delta}}. \\ &= -(k_3 - \frac{\nu_1}{2})\boldsymbol{z}_2^T\boldsymbol{z}_2 - (k_4 - \frac{\nu_2}{2})\boldsymbol{z}_3^T\boldsymbol{z}_3 + \frac{1}{2\nu_1}\|\tilde{\boldsymbol{v}}_d\|^2 \\ &\quad + \frac{1}{2\nu_2}\|\tilde{\boldsymbol{\Delta}}\|^2. \end{aligned} \tag{44}$$

By invoking (36), one has

$$\begin{aligned} \boldsymbol{z}_2^T\boldsymbol{z}_2 &= \boldsymbol{z}_1^T(\mathcal{T}_1 \otimes I_3)^T(\mathcal{T}_1 \otimes I_3)\boldsymbol{z}_1 \\ &= \boldsymbol{z}_1^T(\mathcal{T}_1^T\mathcal{T}_1 \otimes I_3)\boldsymbol{z}_1 \\ &\geq \lambda_{\min}^2(\mathcal{T}_1)\boldsymbol{z}_1^T\boldsymbol{z}_1 \\ &= \frac{\lambda_{\min}^2(\mathcal{T}_1)}{\lambda_{\max}(\mathcal{T}_1)}\lambda_{\max}(\mathcal{T}_1)\boldsymbol{z}_1^T\boldsymbol{z}_1 \\ &\geq \frac{\lambda_{\min}^2(\mathcal{T}_1)}{\lambda_{\max}(\mathcal{T}_1)}\boldsymbol{z}_1^T(\mathcal{T}_1 \otimes I_3)\boldsymbol{z}_1 \\ &= 2\frac{\lambda_{\min}^2(\mathcal{T}_1)}{\lambda_{\max}(\mathcal{T}_1)}V_2. \end{aligned} \tag{45}$$

Now (44) becomes

$$\dot{V}_3 \leq -\varrho V_3 + \delta, \tag{46}$$

where

$$\varrho := \min\{(2k_3 - \nu_1)\lambda_{\min}^2(\mathcal{T}_1)/\lambda_{\max}(\mathcal{T}_1), 2k_4 - \nu_2\}$$
$$\delta := \frac{1}{2\nu_1}\zeta_1^2 + \frac{1}{2\nu_2}\zeta_2^2. \tag{47}$$

From [48], we know $\boldsymbol{z}_1$ and $\boldsymbol{z}_3$ are bounded. This completes the proof. □

3.4. *Modified controller for safety certificates*

Quadrotor team is a safety-critical system. The proposed nominal controller has achieved tracking performance at steady states. However, the system's safety at transient state cannot be guaranteed. Moreover, the control input constraint (8) is not considered in (41) too. In this section, we design a scheme based on ECBF such that the constraints (7) and (8) are strictly enforced.

From safety constraint (7), we can derive

$$x_{ij}^T(\Lambda^{-1})^2 x_{ij} - D_s^2 \geq 0, \tag{48}$$

where $x_{ij} = x_i - x_j$ is the relative position for a pairwise UAVs. Then we can define a pairwise safety set

$$\mathcal{C}_{ij} = \{x_i \in \mathbb{R}^3 | x_{ij}^T(\Lambda^{-1})^2 x_{ij} - D_s^2 \geq 0\}. \quad \forall j \neq i. \tag{49}$$

The overall safety space $\mathcal{C}$ of the system is

$$\mathcal{C} = \prod_i \left\{ \bigcap_{j\neq i} \mathcal{C}_{ij} \right\} \tag{50}$$

where the product represents the Cartesian product.

Now, the collision avoidance between the pairwise quadrotors can be enforced through the forward invariance of the safety set. Denote $h_{ij} = x_{ij}^T(\Lambda^{-1})^2 x_{ij} - D_s^2$, and we choose h_{ij} as an ECBF candidate. For the dynamic system (2), the control input u_i appears as the second derivative of x_i. Therefore, the relative degree of h_{ij} is 2. By combining (12), there are constraints the candidate function needs to satisfy

$$\ddot{h}_{ij} + K[h_{ij}, \dot{h}_{ij}]^T \geq 0. \tag{51}$$

According to (13), the closed loop matrix A_s of a second-order system is given by

$$A_s = \begin{bmatrix} 0 & 1 \\ 0 & 0 \end{bmatrix} - \begin{bmatrix} 0 \\ 1 \end{bmatrix} K \tag{52}$$

where K can be calculated through placing the poles of A_s to negative real parts.

By taking the derivative of h_{ij}, we have

$$\dot{h}_{ij} = 2x_{ij}^T(\Lambda^{-1})^2 v_{ij}. \tag{53}$$

$$\ddot{h}_{ij} = 2v_{ij}^T(\Lambda^{-1})^2 v_{ij} + 2x_{ij}^T(\Lambda^{-1})^2 \dot{v}_{ij}, \tag{54}$$

where $v_{ij} = v_i - v_j$ is the relative velocity. Furthermore, we have

$$\begin{aligned} \dot{v}_{ij} &= \dot{v}_i - \dot{v}_j \\ &= (u_i + \bar{\boldsymbol{g}} + \rho_i v_i + \Delta_i) - (u_i + \bar{\boldsymbol{g}} + \rho_j v_j + \Delta_j) \\ &= (u_i - u_j) + (\rho_i v_i - \rho_j v_j) + (\Delta_i - \Delta_j). \end{aligned} \tag{55}$$

We can find that $\ddot{\boldsymbol{h}}_{ij}$ is affine in u_i, u_j. By substituting (53) and (54) into (51), we obtain

$$A_{ij}(u_i - u_j) \leq b_{ij}, \quad j \neq i, \tag{56}$$

where $A_{ij} = -2x_{ij}^T(\Lambda^{-1})^2$, and

$$\begin{aligned} b_{ij} = {} & K[h_{ij}, \dot{h}_{ij}]^T + 2v_{ij}^T(\Lambda^{-1})^2 v_{ij} - A_{ij}(\rho_i v_i - \rho_j v_j) \\ & - A_{ij}(\Delta_i - \Delta_j). \end{aligned} \tag{57}$$

Owing to the existence of bounded uncertainty and disturbance, we denote

$$\begin{aligned} \bar{b}_{ij} = {} & K[h_{ij}, \dot{h}_{ij}]^T + 2v_{ij}^T(\Lambda^{-1})^2 v_{ij} - A_{ij}(\rho_i v_i - \rho_j v_j) \\ & - 2\|A_{ij}\| \bar{\Delta}. \end{aligned} \tag{58}$$

According to (20), after finite time T_1, $\bar{\Delta}$ can be replaced by ζ_1.

Then we modify (56) into

$$A_{ij}(u_i - u_j) \leq \bar{b}_{ij}, \quad j \neq i. \tag{59}$$

Obviously, $b_{ij} \geq \bar{b}_{ij}$, $A_{ij} = -A_{ji}$, $\bar{b}_{ij} = \bar{b}_{ji}$. We can partition the coupled pairwise constraint (59) into a decentralized form for each individual quadrotor

$$\begin{aligned} A_{ij}u_i &\leq \frac{\alpha_i}{\alpha_i + \alpha_j}\bar{b}_{ij}, \\ A_{ji}u_j &\leq \frac{\alpha_j}{\alpha_i + \alpha_j}\bar{b}_{ji}. \end{aligned} \tag{60}$$

In this paper, we suppose that all quadrotors are homogeneous with the same maneuver capabilities. Therefore, we have $\alpha_i = \cdots = \alpha_j = \cdots = \alpha$. Then (60) becomes

$$\begin{aligned} A_{ij}u_i &\leq \frac{1}{2}\bar{b}_{ij}, \\ A_{ji}u_j &\leq \frac{1}{2}\bar{b}_{ji}. \end{aligned} \tag{61}$$

Based on the safety constraint (61), the nominal controller should be modified for the safety certificates. We hope that the modification has minimal violation of $\bar{u}_i$. In the sense of least squares, the optimal control input u_i^* can be obtained

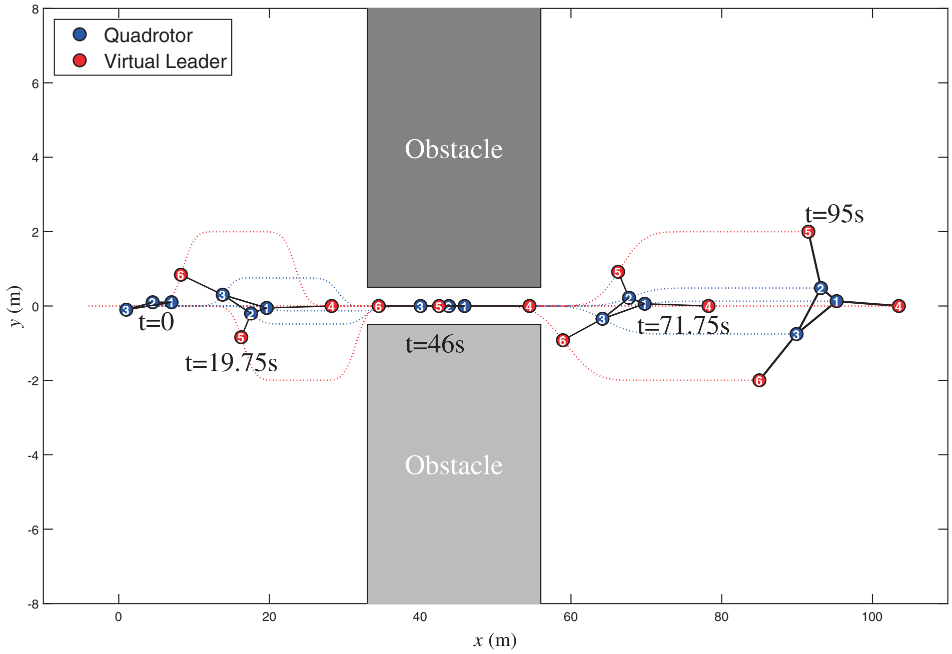

Fig. 2. View of the trajectories and formations in x-y plane.

through solving a quadratic programming (QP) problem, in which the input constraint (8) is also considered.

Based on the above statement, the methodology is summarized and given in the following algorithm.

Algorithm 3.5. The controller based on ECBF-QP can be obtained in the following:

$$\begin{aligned} u_i^* &= \underset{u_i}{\operatorname{argmin}} \|u_i - \bar{u}_i\|^2 \\ \text{s.t.} \quad & A_{ij} u_i \leq \frac{1}{2} \bar{b}_{ij}, \quad i, j \in F, \ \forall j \neq i \\ & \|u_i\|_\infty \leq \alpha, \quad i \in F. \end{aligned} \tag{62}$$

Through this algorithm, the modified control input u_i^* guarantees the hard constraints (7) and (8) strictly. If there is contradiction between hard constraints and tracking constraint, the optimal controller's deviation form $\bar{u}_i$ is as small as possible. That is a trade-off.

4. Simulation Examples

In this section, numerical simulation examples are given to illustrate the effectiveness of the proposed control scheme.

We construct a system consisting of 3 quadrotors (labeled as 1, 2, 3) and 3 virtual leaders (labeled as 4, 5, 6), the communication topology is described in Fig. 3.

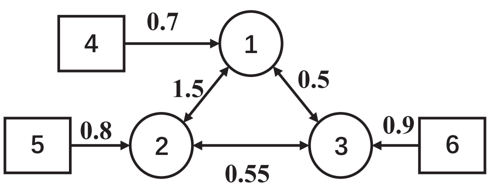

Fig. 3. Communication topology.

4.1. *Case 1: The nominal controller*

In the first simulation example, the nominal controller is applied on the quadrotors. Leaders' formation keeps maneuvering in the environment. The formation will reconfigure when in need. It can scale down to across a narrow corridor and then recover. The quadrotors should follow the leaders, track the desired trajectory to stay in the convex hull.

The parameters of quadrotors are set as $m_i = 0.3\,\text{kg}$, $g = 9.8\,\text{m/s}^2$, $\bar{r} = 3.5$. Parameters to be designed are given by $k_1 = 1$, $k_2 = 4$, $a = 2$, $\nu_1 = \nu_2 = 1$, $k_3 = 3$, $k_4 = 3$. The initial conditions are set as $x_1(0) = [7, 0.1, 9.8]^T$, $x_2(0) = [4.5, 0.1, 9.8]^T$, $x_3(0) = [1, -0.1, 10.1]^T$. $p_4(0) = [14, 0, 10]^T$, $p_5(0) = [4, 0, 10]^T$, $p_6(0) = [-4, 0, 10]^T$. $v_1(0) = v_2(0) = v_3(0) = q_4(0) = q_5(0) = q_6(0) = [0, 0, 0]^T$.

For simplicity, only the trajectories and formations in x–y plane are shown in Fig. 2. We can find that the quadrotors' formation maneuver control is achieved through the

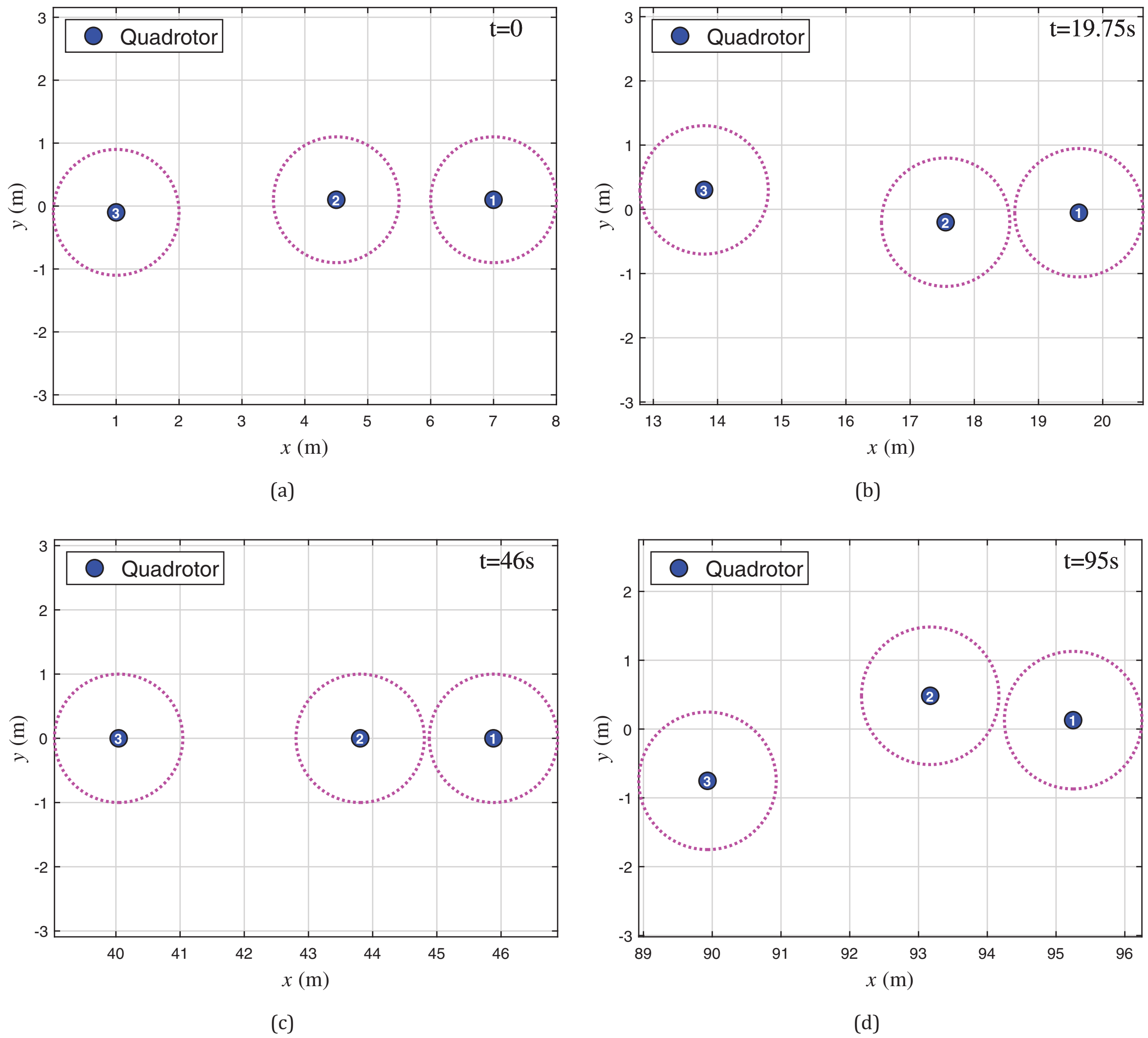

Fig. 4. Collision detection at (a) $t = 0$, (b) $t = 19.75s$, (c) $t = 46s$, (d) $t = 95s$.

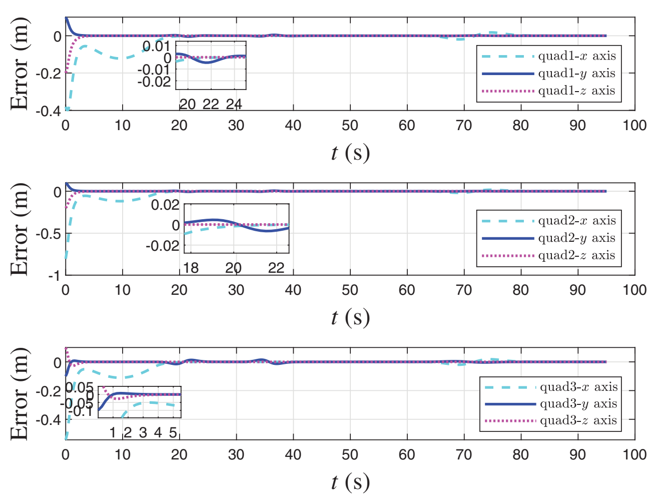

Fig. 5. Tracking error of 3 quadrotors with nominal controller.

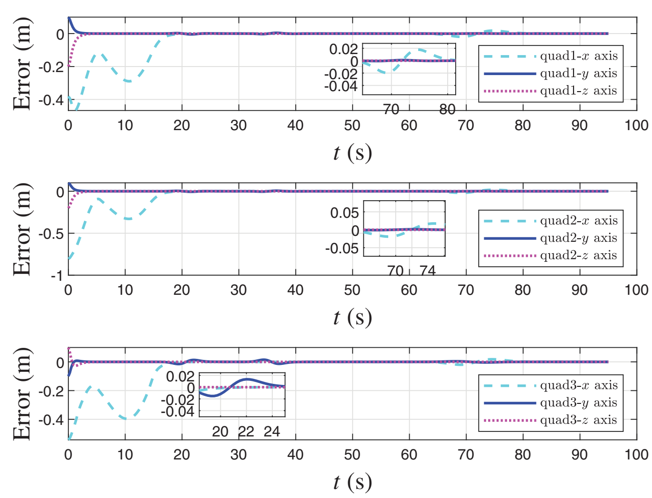

Fig. 6. Tracking error of 3 quadrotors with ECBF-QP.

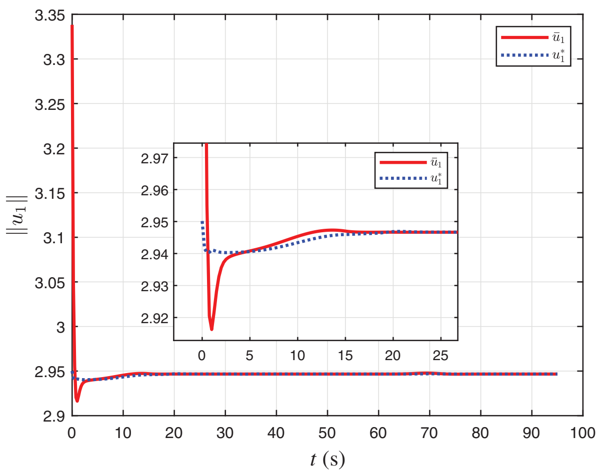

(a)

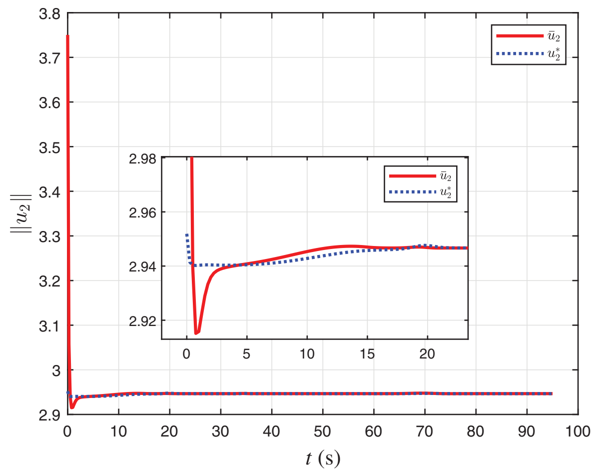

(b)

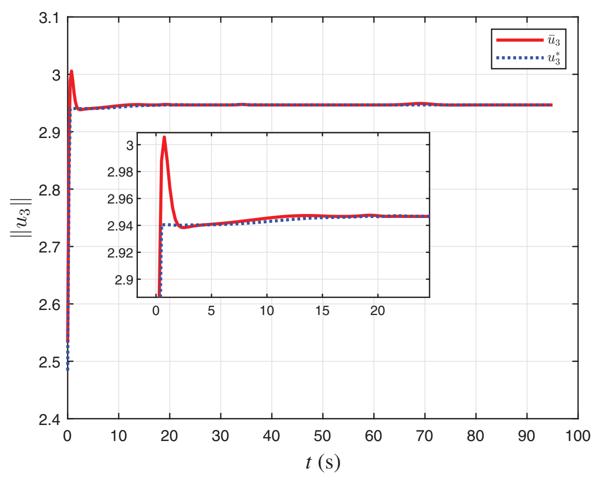

(c)

Fig. 7. Control input of (a) quadrotor 1; (b) quadrotor 2; (c) quadrotor 3.

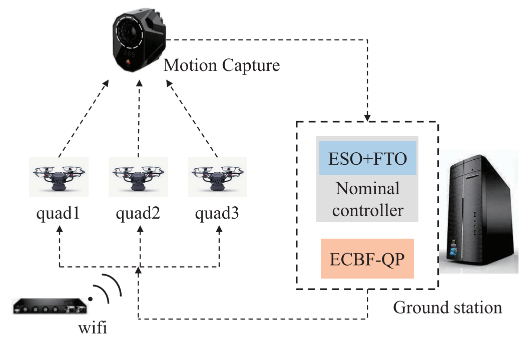

Fig. 8. Experiment setup.

containment of the virtual leaders. Three quadrotors form a queue to pass through the narrow corridor successfully. The tracking errors for 3 quadrotors are shown in Fig. 5, respectively.

It can be seen the errors will converge and remain close to 0 after formation maneuver such that the constraint (6) is satisfied.

4.2. *Case 2: Modified controller with safety certificates*

Based on the first example, we add safety-critical constraint to the nominal controller. The parameters and initial conditions are the same as those in case 1. In (52), by placing the eigenvalues of A_s at $-1, -2$, we have $K = [2, 3]$. Then we construct a QP problem (62), in which the safety distance $D_s = 2$ m, scaling matrix $\Lambda = \mathrm{diag}\{1, 1, 1.5\}$.

After employing the modified controller, we detect the potential collision in the whole simulation process, the results are shown in Fig. 4. The collision between the

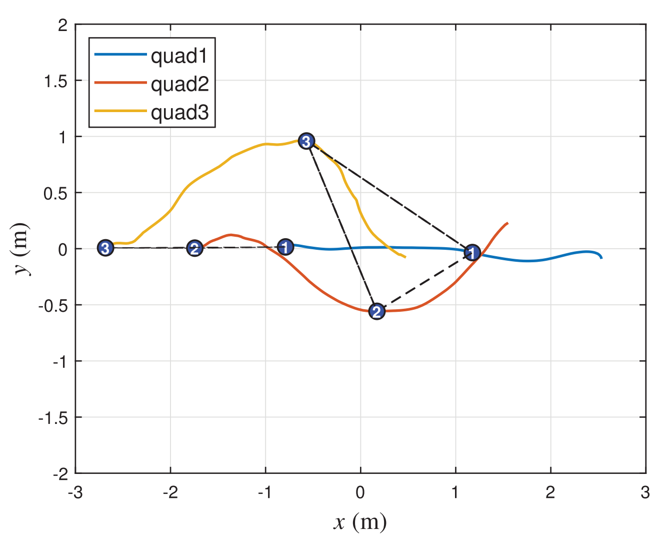

Fig. 9. Flight trajectories.

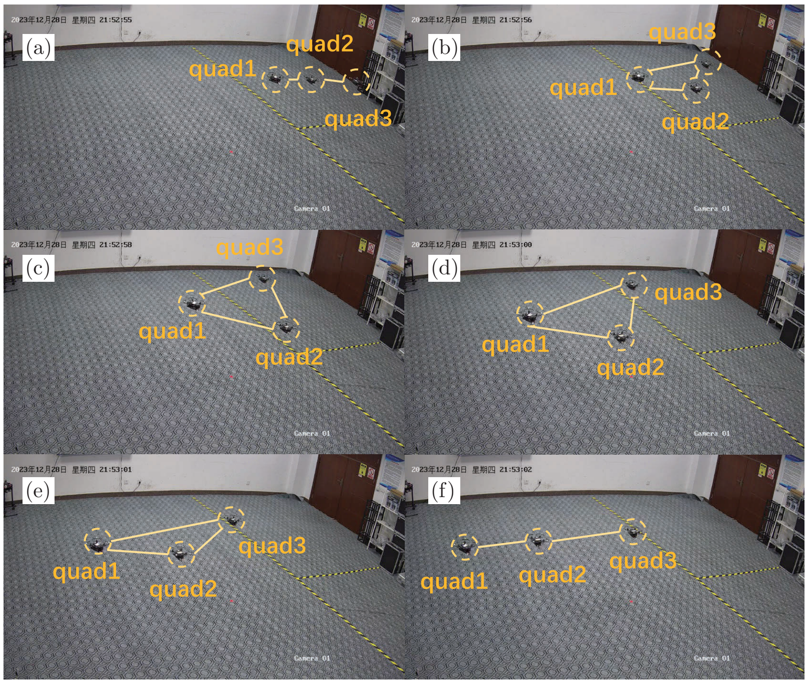

Fig. 10. Key frames in experiment.

quadrotors is successfully avoided such that the control objective (7) is achieved. Figure 6 shows the tracking error of quadrotors using new controllers. It can be seen that although the nominal controller is modified, the tracking performance can still be guaranteed, which means constraint (6) still holds.

Finally, we make a comparison of the two proposed controllers, which is shown in Fig. 7. We can see that the nominal controller may violate the limit of control input sometimes, the input constraint can be satisfied using the modified controller.

5. Experiment

We test our algorithm through a actual flight experiment. Setup of the indoor experiment is displayed in Fig. 8.

Similar to simulation examples, we use 3 Pixhawk quadrotors (quad1, quad2, quad3) for formation maneuvering. Indoor positioning is realized via a motion capture system. Computation of the algorithm is running on a ground station PC in real time. The signals are transmitted through wireless communication.

Admissible flight space in our lab is $8\,\mathrm{m} * 8\,\mathrm{m}$. Safety distance D_s is set as $0.8\,\mathrm{m}$ and the input constraint $\alpha = 1.5$.

Three quadrotors were arranged randomly on the ground. At the beginning, they took off vertically and assembled to form a straight line pattern. Then they started to move forward and maneuver into a triangular pattern. In the end, the quadrotors' configuration changed back to the straight line and landed. During the experiment, we also turned on the fan in the room to simulate the external disturbance.

The trajectories during the flight process are displayed in Fig. 9.

We also take a video to record the experiment. Then we extract 6 key frames from the video and demonstrate them in Fig. 10.

It can be seen that the quadrotors complete the task successfully. The result is generally satisfactory, which shows the effectiveness of our algorithm.

6. Conclusion

This work aims at the containment control for quadrotor teams under multiple constraints. The proposed algorithm can be summarized as 2 steps. One is an ESO and FTO-based backstepping nominal controller, another one is an ECBF-QP-based optimization. Some simulation examples and flight experiment are presented to validate the proposed control scheme. In future work, we will study the heterogeneous system and conduct our experiment in a more complex environment. How to avoid the deadlock phenomenon of ECBF is also a challenge, which deserves more attention.

ORCID

Zheng Xia https://orcid.org/0009-0001-1987-4483
Mou Chen https://orcid.org/0000-0001-7158-8575

References

[1] T. T. Nguyen, N. D. Nguyen and S. Nahavandi, Deep reinforcement learning for multiagent systems: A review of challenges, solutions, and applications, *IEEE Trans. Cybern.* **50**(9) (2020) 3826–3839.
[2] H. Li and X. Li, Finite-time predictive consensus for discrete-time heterogeneous multi-agent systems over switching digraphs, *IEEE Trans. Circuits Syst. II: Exp. Briefs* **70**(6) (2023) 2136–2140.
[3] L. A. Dennis and M. Fisher, Verifiable self-aware agent-based autonomous systems, *Proc. IEEE* **108**(7) (2020) 1011–1026.
[4] N. Gu, D. Wang, Z. Peng, J. Wang and Q.-L. Han, Advances in line-of-sight guidance for path following of autonomous marine vehicles: An overview, *IEEE Trans. Syst. Man Cybern.: Syst.* **53**(1) (2023) 12–28.
[5] S. Mayya, D. S. D'antonio, D. Saldaña and V. Kumar, Resilient task allocation in heterogeneous multi-robot systems, *IEEE Robot. Autom. Lett.* **6**(2) (2021) 1327–1334.
[6] X. Zhou, X. Wen, Z. Wang, Y. Gao, H. Li, Q. Wang, T. Yang, H. Lu, Y. Cao, C. Xu and F. Gao, Swarm of micro flying robots in the wild, *Sci. Robot.* **7**(66) (2022) eabm5954.
[7] Z. Jiandong, Y. Qiming, S. Guoqing, L. Yi and W. Yong, UAV cooperative air combat maneuver decision based on multi-agent reinforcement learning, *J. Syst. Eng. Electron.* **32**(6) (2021) 1421–1438.
[8] Q. Liu, Z. Nie, Z. Gong and X.-J. Liu, An omnidirectional transportation system with high terrain adaptability and flexible configurations using multiple nonholonomic mobile robots, *IEEE Robot. Autom. Lett.* **8**(9) (2023) 6060–6067.
[9] Y. Zhang, Y. Zhang and Z. Yu, A solution for searching and monitoring forest fires based on multiple UAVs, *2019 Int. Conf. Unmanned Aircraft Systems (ICUAS)* (IEEE, 2019), pp. 661–666.
[10] D. Mellinger and V. Kumar, Minimum snap trajectory generation and control for quadrotors, *2011 IEEE Int. Conf. Robotics and Automation* (IEEE, 2011), pp. 2520–2525.
[11] H. Li and X. Li, Distributed consensus of heterogeneous linear time-varying systems on UAVs–USVs coordination, *IEEE Trans. Circuits Syst. II: Exp. Briefs* **67**(7) (2020) 1264–1268.
[12] X. Hai, H. Qiu, C. Wen and Q. Feng, A novel distributed situation awareness consensus approach for UAV swarm systems, *IEEE Trans. Intell. Transp. Syst.* **24**(12) (2023) 14706–14717.
[13] X. Dong, Y. Zhou, Z. Ren and Y. Zhong, Time-varying formation tracking for second-order multi-agent systems subjected to switching topologies with application to quadrotor formation flying, *IEEE Trans. Indust. Electron.* **64**(6) (2017) 5014–5024.
[14] H. Cao, L. Han, D. Li, Q. Hu and P. Hao, Fully distributed dynamic event-triggering formation control of UAV swarms under dos attacks, *2023 62nd IEEE Conference on Decision and Control (CDC)* (IEEE, 2023), pp. 3166–3173.
[15] Q. Yang, M. Cao, H. Fang and J. Chen, Constructing universally rigid tensegrity frameworks with application in multiagent formation control, *IEEE Trans. Autom. Control* **64**(1) (2019) 381–388.
[16] F. Xiao, Q. Yang, X. Zhao and H. Fang, A framework for optimized topology design and leader selection in affine formation control, *IEEE Robot. Autom. Lett.* **7**(4) (2022) 8627–8634.
[17] M. Ranjbar, M. T. H. Beheshti and S. Bolouki, Event-based formation control of networked multi-agent systems using complex Laplacian under directed topology, *IEEE Control Syst. Lett.* **5**(3) (2021) 1085–1090.
[18] X. Fang and L. Xie, Distributed formation maneuver control using complex Laplacian, *IEEE Trans. Autom. Control* **69**(3) (2024) 1850–1857.
[19] S. Zhao, Affine formation maneuver control of multiagent systems, *IEEE Trans. Autom. Control* **63**(12) (2018) 4140–4155.
[20] Y. Feng, H. Wang and J. Fu, Finite-time event-triggered containment maneuvering of marine surface vehicles with tracking error constraints: Theory and experiment, *IEEE Trans. Intell. Vehicles* (2024) 1–11.
[21] Y. Shi, Y. Hua, J. Yu, X. Dong, J. Lü and Z. Ren, Resilient output formation-containment tracking of heterogeneous multi-agent systems: A learning-based framework using dynamic data, *IEEE Trans. Netw. Sci. Eng.* **11**(4) (2024) 3678–3691.
[22] L. Feng, B. Huang, J. Sun, Q. Sun and X. Xie, Adaptive event-triggered time-varying output group formation containment control of heterogeneous multiagent systems, *IEEE/CAA J. Autom. Sin.* **11**(6) (2024) 1398–1409.
[23] P. Zhou and B. M. Chen, Formation-containment control of Euler–Lagrange systems of leaders with bounded unknown inputs, *IEEE Trans. Cybern.* **52**(7) (2020) 6342–6353.
[24] W. Xi, M. Hu, H. Wang, H. Dong and Z. Ying, Formation control for virtual coupling trains with parametric uncertainty and unknown disturbances, *IEEE Trans. Circuits Syst. II: Exp. Briefs* **70**(9) (2023) 3429–3433.
[25] X. Ge and Q.-L. Han, Distributed formation control of networked multi-agent systems using a dynamic event-triggered communication mechanism, *IEEE Trans. Indust. Electron.* **64**(10) (2017) 8118–8127.
[26] H. Xu, G. Cui, Q. Ma and Z. Li, Event-triggered distributed adaptive fixed-time formation control of QUAVs with input constraints, *IEEE Trans. Vehicul. Technol.* **73**(5) (2024) 6357–6367.
[27] J. Fu, G. Wen, X. Yu and T. Huang, Robust collision-avoidance formation navigation of velocity and input-constrained multirobot systems, *IEEE Trans. Cybern.* **54**(3) (2024) 1734–1746.
[28] X. Wang, B. Niu, H. Wang, X. Zhao and W. Chen, Prescribed performance-based finite-time consensus technology of nonlinear multiagent systems and application to FDPs, *IEEE Trans. Circuits Syst. II: Exp. Briefs* **70**(2) (2022) 591–595.
[29] Y.-J. Liu, S. Lu, S. Tong, X. Chen, C. P. Chen and D.-J. Li, Adaptive control-based barrier Lyapunov functions for a class of stochastic nonlinear systems with full state constraints, *Automatica* **87** (2018) 83–93.
[30] J. Zeng, B. Zhang and K. Sreenath, Safety-critical model predictive control with discrete-time control barrier function, *2021 American Control Conf. (ACC)* (IEEE, 2021), pp. 3882–3889.
[31] Y. Lyu, J. Hu, B. M. Chen, C. Zhao and Q. Pan, Multivehicle flocking with collision avoidance via distributed model predictive control, *IEEE Trans. Cybern.* **51**(5) (2019) 2651–2662.
[32] J. A. Preiss, W. Hönig, N. Ayanian and G. S. Sukhatme, Downwash-aware trajectory planning for large quadrotor teams, *2017 IEEE/RSJ Int. Conf. Intelligent Robots and Systems (IROS)* (IEEE, 2017), pp. 250–257.
[33] N. Gu, D. Wang, Z. Peng and L. Liu, Observer-based finite-time control for distributed path maneuvering of underactuated unmanned surface vehicles with collision avoidance and connectivity preservation, *IEEE Trans. Syst. Man Cybern.: Syst.* **51**(8) (2019) 5105–5115.
[34] A. D. Ames, X. Xu, J. W. Grizzle and P. Tabuada, Control barrier function based quadratic programs for safety critical systems, *IEEE Trans. Autom. Control* **62**(8) (2016) 3861–3876.
[35] J. Fu, G. Wen, X. Yu and Z.-G. Wu, Distributed formation navigation of constrained second-order multiagent systems with collision avoidance and connectivity maintenance, *IEEE Trans. Cybern.* **52**(4) (2020) 2149–2162.

[36] N. Gu, D. Wang, Z. Peng and J. Wang, Safety-critical containment maneuvering of underactuated autonomous surface vehicles based on neurodynamic optimization with control barrier functions, *IEEE Trans. Neural Netw. Learn. Syst.* **34** (2021) 2882–2895.
[37] Q. Nguyen and K. Sreenath, Exponential control barrier functions for enforcing high relative-degree safety-critical constraints, *2016 American Control Conference (ACC)* (IEEE, 2016), pp. 322–328.
[38] L. Wang, A. D. Ames and M. Egerstedt, Safety barrier certificates for collisions-free multirobot systems, *IEEE Trans. Robot.* **33**(3) (2017) 661–674.
[39] T. Lee, M. Leok and N. H. McClamroch, Geometric tracking control of a quadrotor UAV on SE (3), *49th IEEE Conf. Decision and Control (CDC)* (IEEE, 2010), pp. 5420–5425.
[40] E. Tal and S. Karaman, Accurate tracking of aggressive quadrotor trajectories using incremental nonlinear dynamic inversion and differential flatness, *IEEE Trans. Control Syst. Technol.* **29**(3) (2020) 1203–1218.
[41] W. Hönig, J. A. Preiss, T. K. S. Kumar, G. S. Sukhatme and N. Ayanian, Trajectory planning for quadrotor swarms, *IEEE Trans. Robot.* **34**(4) (2018) 856–869.
[42] X. Dong, Y. Hua, Y. Zhou, Z. Ren and Y. Zhong, Theory and experiment on formation-containment control of multiple multirotor unmanned aerial vehicle systems, *IEEE Trans. Autom. Sci. Eng.* **16**(1) (2019) 229–240.
[43] Z. Meng, W. Ren and Z. You, Distributed finite-time attitude containment control for multiple rigid bodies, *Automatica* **46**(12) (2010) 2092–2099.
[44] W. Cheng, K. Zhang and B. Jiang, Fixed-time and prescribed-time fault-tolerant optimal tracking control for heterogeneous multiagent systems, *IEEE Trans. Autom. Sci. Eng.* **21**(4) (2023) 7275–7286.
[45] C. Hu and H. Jiang, Special functions-based fixed-time estimation and stabilization for dynamic systems, *IEEE Trans. Syst. Man Cybern.: Syst.* **52**(5) (2022) 3251–3262.
[46] J. Yue, Z. Liu and H. Su, Model-free composite disturbance rejection control for dynamic wireless charging system based on online parameter identification, *IEEE Trans. Indust. Electron.* **71**(7) (2024) 7777–7785.
[47] H. Cao, Y. Li, C. Liu and S. Zhao, ESO-based robust and high-precision tracking control for aerial manipulation, *IEEE Trans. Autom. Sci. Eng.* **21**(2) (2024) 2139–2155.
[48] M. Chen, P. Shi and C.-C. Lim, Adaptive neural fault-tolerant control of a 3-dof model helicopter system, *IEEE Trans. Syst. Man Cybern.: Syst.* **46**(2) (2015) 260–270.